

# A preliminary comparison between finite element and meshless simulations of extrusion

L. Filice<sup>a</sup> I. Alfaro<sup>b</sup> F. Gagliardi<sup>a</sup> E. Cueto<sup>b,\*</sup> F. Micari<sup>c</sup>  
F. Chinesta<sup>d</sup>

<sup>a</sup>*Dept. of Mechanical Engineering, University of Calabria, 87036 Rende - Italy*

<sup>b</sup>*Aragon Institute of Engineering Research, University of Zaragoza. 50018 Zaragoza, Spain*

<sup>c</sup>*Dept. of Technology, Production and Management Eng., University of Palermo, 90126 Palermo - Italy*

<sup>d</sup>*LMSP UMR 8106 CNRS-ENSAM-ESEM. École Nationale Supérieure d'Arts et Métiers. 75013 Paris, France*

---

## Abstract

In this paper the extrusion process of a cross-shaped profile was investigated. In particular, the study was focused on the distortion of extruding profiles when the workpiece and die axis are not aligned. The process was simulated using the Finite Element Method (FEM) and the Natural Element Method (NEM), both implemented in an updated-Lagrangian formulation, in order to avoid the burden associated with the description of free surfaces in ALE or Eulerian formulations. Furthermore, an experimental equipment was developed in order to obtain reliable data in terms of deformed entity, required process load and calculated pressure. At the end, a comparison between the numerical predictions and the experimentally measured data was carried out. The main results are presented in the paper.

*Key words:* Meshless methods, NEM, FEM, Extrusion.

---

\* Corresponding author. Address: Aragon Institute of Engineering Research. University of Zaragoza. Edificio Betancourt. Campus Rio Ebro. María de Luna, s.n. E-50018 Zaragoza, Spain.

*Email address:* [ecueto@unizar.es](mailto:ecueto@unizar.es) (E. Cueto).

## 1 Introduction

Extrusion is one of the most utilised bulk metal forming processes. It is particularly suitable when high reductions in area are required or when hollow components have to be manufactured. Extrusion analysis has been carried out, in the past, utilising some analytical techniques based on the slab method although such approach results applicable only if simple geometries are taken into account. The introduction of Finite Elements and, in particular, the development of efficient mesh management procedures, allowed the simulation of very complex processes characterised by large surfaces generation, high strains and strain rates.

Up to now, the most relevant limitation is associated with the numerical dissipation introduced with remeshing procedures. When the mesh becomes too distorted in a particular domain, a new mesh must be generated and the variables associated with material history must be mapped from the old mesh to the new. This introduces additional errors that meshless formulation can avoid. On the other hand, the simulation of hollow components extrusion introduces another critical aspect since material joining (after the previous separation in correspondence of the porthole) has to be properly modelled. According to the above considerations, the development of a new modelling technique able to introduce a sort of discontinuity with respect to the currently applied ones can be strategic.

Very few examples exist of the application of meshless methods to the simulation of forming processes, and none (up to our knowledge) to extrusion. Nevertheless, we can cite the pioneering work by Chen *et al.* (1998) as one of the earliest examples, together with (Bonet and Kulasegaram, 2000). They use, however, early implementation of meshless methods that still have some drawbacks. One of the most important is the lack of proper interpolation on the boundary. This produces some problems in the correct imposition of essential boundary conditions and, of course, in the appropriate simulation of contact and friction.

In this paper a well established meshless technique known as Natural Element Method (NEM, (Sukumar *et al.*, 1998)) is adapted to the simulation of extrusion processes. The NE technique presents some advantages over Finite Element simulations: no remeshing is necessary since a satisfactory accuracy of the approximation is achieved even with highly distorted triangles or tetrahedra. The price to pay is, obviously, a higher computational cost. The method is here employed in conjunction with the notion of  $\alpha$ -shapes of the cloud of nodes in order to extract the geometry of the extruded part as it evolves. This state-of-the-art geometrical concept allows to avoid complex geometrical checks of self-contact on the boundary of the domain, as shown by Alfaro *et al.*

(2006a) or Alfaro *et al.* (2006b).

In the study here addressed a simple 3-D extrusion process was taken into account, characterised by an asymmetric die which determines a distortion of the extruded profile. The study of profile distortion is important for practical purposes of real-life extrusions, but also to test the geometrical algorithms employed to track the free surfaces in the simulation. As far as the proposed approach is concerned, home-made FE and NE codes were utilised for the process modelling. In order to analyse the origins of possible discrepancies between both techniques, the heat generation due to plastic deformation has been neglected, although it can be considered without any limitations to the technique, as in some of our previous works, see for instance (Alfaro *et al.*, 2006a) or (Alfaro *et al.*, 2006b). Finally, a proper experimental equipment was developed. The numerical results were compared to the experimental evidences taking into account some interesting process variables, namely the required process load, the pressure on the die and the geometry of the extruded profile.

## 2 The case under study

### 2.1 Constitutive modelling

The process geometrical data are reported in Fig. 1. The chosen material for all the tests is UNS L51120 chemical Lead, due to its property to yield at room temperature with moderate loads. Its behaviour was modelled through a power-law type constitutive equation, reported in Eq. (1).

$$\sigma = 60\dot{\epsilon}^{0.05} \text{ in MPa} \quad (1)$$

More in detail, three sets of upsetting tests were carried out on cylindrical specimens, reducing as much as possible the friction between the basis and the press-plates. The tests were carried out utilising an Instron 8501 electronically controlled hydraulic testing machine and the average strain rate was fixed as  $0.05s^{-1}$  (hence, quasi-static),  $50s^{-1}$  and  $100s^{-1}$  in order to range into a wide area. Results are depicted in Fig. 2. The flow rule was derived by using an inverse approach based on the predicted data of a simple numerical simulation. To this end, a general visco-plastic Norton-Hoff law was adjusted with the experimental data.

The general Norton-Hoff visco-plastic model can be stated as

$$\boldsymbol{\sigma}^{dev} = \frac{2}{3d} \mu_0 (\sqrt{3})^{n+1} e^{\beta T} \bar{d}^n \bar{\epsilon}^h \mathbf{d} \quad (2)$$

where the superscript  $dev$  refers to the deviatoric part of the stress tensor,  $\bar{d}$  represents the equivalent strain rate, and  $n$ ,  $h$  and  $\beta$  are parameters of the model. We have neglected the dependence of the model with temperature and strain, assuming dependence on strain rate only. After particularising this model for the uniaxial case, we arrive to  $\mu_0 = 33.70$  and  $n = 0.05$ .

We thus obtain a rigid visco-plastic model (similar to the *flow formulation* by Zienkiewicz and Godbolet (1974)) in the form

$$\boldsymbol{\sigma}^{dev} = 2\mu\mathbf{d}, \quad (3)$$

where  $\mu = \frac{2}{3}\mu_0(\sqrt{3})^{n+1}\bar{d}^{n-1}$ .

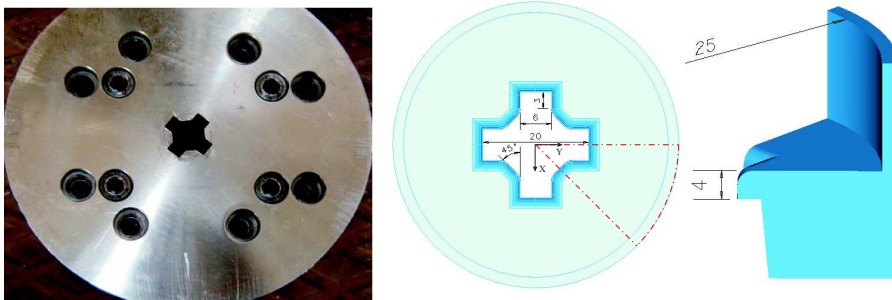


Fig. 1. Geometry of the die for the experiments (left) and the numerical simulation (right).

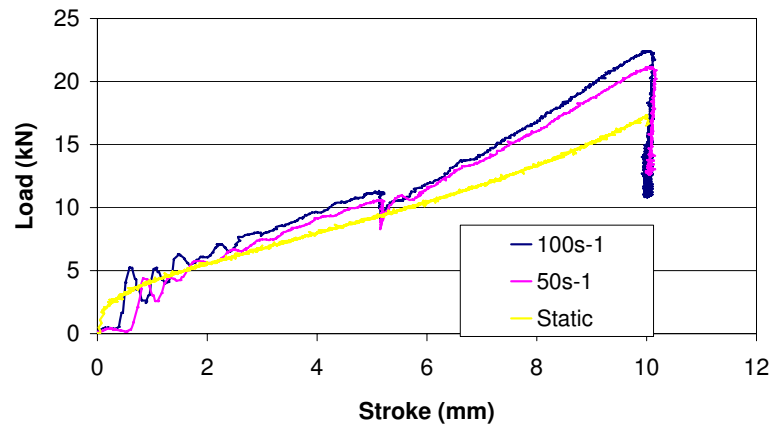


Fig. 2. Evolution of punch load during the characterisation essays.

The requested process load and the shape of the obtained extruded profiles were measured. In particular, a configuration with an asymmetric die with 10

mm of misalignment (Figs. 1 and 3) was investigated in order to induce the distortion of the extruded profile. The geometry of the profile was obtained after Zhou *et al.* (2003).

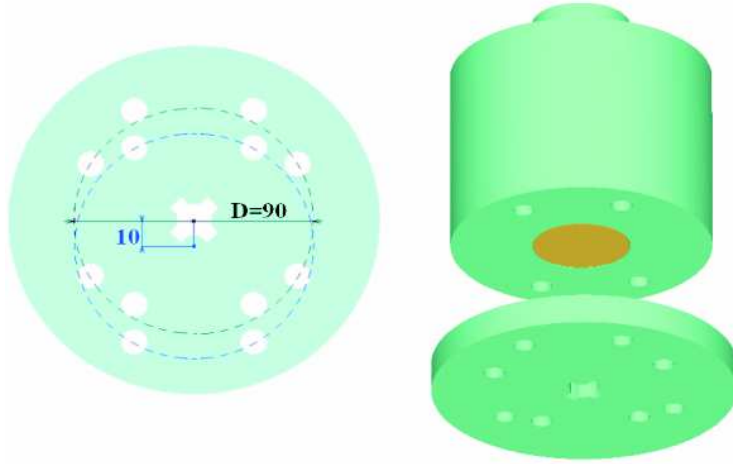


Fig. 3. Sketch of the possible die assemblies with zero or 10 mm of misalignment.

## 2.2 Constitutive modelling of friction

In the simulations here presented, a viscoplastic model for the friction between the lead and the walls of the die was considered. Following the notation established by Chenot *et al.* (2002), the viscoplastic friction law is described by a non-linear constitutive equation, relating the shear stress vector  $\boldsymbol{\tau}$  and the relative velocity between the lead (in this case) and the walls of the die,  $\boldsymbol{v}_s$ :

$$\boldsymbol{\tau} = -\alpha_f(\sigma_n)K|\boldsymbol{v}_s|^{q-1}\boldsymbol{v}_s \quad (4)$$

where  $\sigma_n$  represents the normal stress at the interface.  $\alpha_f$ , the viscoplastic friction coefficient, can be established as a function of the normal stress  $\sigma_n$  (Chenot *et al.*, 2002) and the sensitivity parameter  $q$  is very often taken equal to  $m$ , and thus equal to 0.05.

## 3 Governing equations

We consider the balance of momentum equations, without inertia and mass terms

$$\nabla \cdot \boldsymbol{\sigma} = \mathbf{0}, \quad (5)$$

and the assumed incompressibility of a von Mises-like flow:

$$\nabla \cdot \boldsymbol{v} = 0, \quad (6)$$

where  $\mathbf{v}$  represents the velocity field. The stress-strain rate relationship is given by Eq. (2).

Together with these equations, appropriate boundary conditions are considered:

$$\boldsymbol{\sigma} \cdot \mathbf{n} = \bar{\mathbf{t}} \text{ in } \Gamma_t \quad (7)$$

$$\mathbf{v} = \bar{\mathbf{v}} \text{ in } \Gamma_v \quad (8)$$

where  $\Gamma_t$  and  $\Gamma_v$  represent, respectively, the part of the boundary  $\Gamma = \partial\Omega$  where tractions and velocities are prescribed.

If we write the incremental variational equation at time  $t + \Delta t$  we arrive to:

$$\int_{\Omega(t+\Delta t)} \left( - (p^t + \Delta p) \mathbf{I} + 2\mu(\mathbf{d}^t + \Delta \mathbf{d})(\mathbf{d}^t + \Delta \mathbf{d}) \right) : \mathbf{d}^* d\Omega = 0 \quad (9)$$

Domain updating is done in an explicit procedure, given the last converged velocity field, but due to the non-linear character of the constitutive equations, an iterative approach has been applied to the conservation equations, using the Newton-Raphson scheme, thus leading to

$$\begin{aligned} \int_{\Omega(t+\Delta t)} \left( - \Delta \Delta p \mathbf{I} + 2\mu \left( \frac{\partial \mu(\mathbf{d}_k^{t+\Delta t})}{\partial \mathbf{d}} : \Delta \Delta \mathbf{d} \right) \mathbf{d}_k^{t+\Delta t} + \right. \\ \left. + 2\mu(\mathbf{d}_k^{t+\Delta t}) \Delta \Delta \mathbf{d} \right) : \mathbf{d}^* d\Omega = \\ = - \int_{\Omega(t+\Delta t)} (-p_k^{t+\Delta t} \mathbf{I} + 2\mu(\mathbf{d}_k^{t+\Delta t}) \mathbf{d}_k^{t+\Delta t}) : \mathbf{d}^* d\Omega \end{aligned} \quad (10)$$

where the subscript  $k$  indicates the iteration within a time increment. The incremental form of the incompressibility condition results

$$\int_{\Omega(t+\Delta t)} \nabla \cdot (\Delta \Delta \mathbf{v}) p^* d\Omega = - \int_{\Omega(t+\Delta t)} \nabla \cdot (\mathbf{v}_k^{t+\Delta t}) p^* d\Omega \quad (11)$$

If we approximate the velocities and pressures, as well as their variations, by employing a finite-dimensional set of basis functions, we arrive to a discrete form of the previous equations (Bubnov-Galerkin method)

$$\Delta \Delta \mathbf{v}^h(\mathbf{x}) = \sum_{I=1}^n \phi_I(\mathbf{x}) \Delta \Delta \mathbf{v}_I \quad (12)$$

$$\Delta \Delta p^h(\mathbf{x}) = \sum_{I=1}^n \psi_I(\mathbf{x}) \Delta \Delta p_I. \quad (13)$$

where  $n$  represents the number of nodes considered in the approximation. The functions  $\psi_I(\mathbf{x})$  and  $\phi_I(\mathbf{x})$  in this work represent some form of finite element (piece-wise polynomials) or natural neighbour interpolation, which will be studied in the following section. This leads to the linear system:

$$\begin{pmatrix} \mathbf{K}_k^{t+\Delta t} & \mathbf{G} \\ \mathbf{G}^T & \mathbf{0} \end{pmatrix} \begin{pmatrix} \Delta\Delta\mathbf{v} \\ \Delta\Delta p \end{pmatrix} = \begin{pmatrix} \mathbf{f}_k^{t+\Delta t} \\ \mathbf{0} \end{pmatrix} \quad (14)$$

being the updating given by

$$\mathbf{v}_{k+1}^{t+\Delta t} = \mathbf{v}_k^{t+\Delta t} + \Delta\Delta\mathbf{v} \quad (15)$$

$$p_{k+1}^{t+\Delta t} = p_k^{t+\Delta t} + \Delta\Delta p \quad (16)$$

Obviously, Eqs. (10) and (11) will be solved iteratively until convergence. The convergence is assumed once the relative modulus of the residual gets under  $10^{-6}$  and the relative increment of the velocity norm is below 0.02.

## 4 Numerical modelling of the extrusion process

### 4.1 Finite Element analysis

From the FE point of view, a linear velocity-constant pressure mixed formulation, based on four node tetrahedra, was employed. This simple formulation possesses obvious limitations (noteworthy some tendency to lock) but presents the same structure as the implemented NE formulation, and the same degrees of freedom per node. Thus it is in the opinion of the authors the most appropriate in order to make a comparison with the NEM results. Despite the lack of compliance with the LBB condition, no locking was observed during the simulations. It should be highlighted, in addition, that the FE formulation employed here is by no means standard in the sense that the FE nodes remain the same throughout the simulation. In this way, no projection of variables is made. This is not frequent in commercial FE codes. At each time step a Delaunay triangulation is performed in the FE nodes, even if it is well-know that the Delaunay triangulation is mainly used in 2D applications.

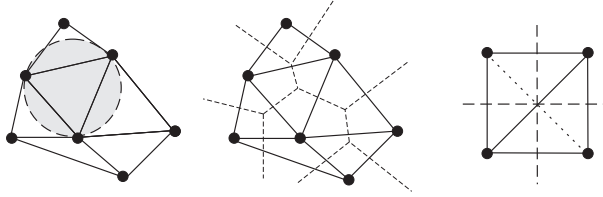


Fig. 4. Delaunay triangulation and Voronoi diagram of a cloud of points.

#### 4.2 Natural neighbour approximations

We review here with some more details the basics of the natural element method, since it is a technique much less known than the finite element method. The vast majority of meshless methods are based on the employ of scattered data approximation techniques to construct the approximating spaces of the Galerkin method. These techniques must have, of course, low sensitivity to mesh distortion, as opposed to FE methods. Among these techniques, the Natural Element Method employs any instance of Natural Neighbour interpolation (Sibson, 1981; Hiyoshi and Sugihara, 1999) to construct trial and test functions. Prior to the introduction of these interpolation techniques, it is necessary to define some basic concepts.

The model will be constructed upon a cloud of points with no connectivity on it. We will call this cloud of points  $\mathbf{N} = \{n_1, n_2, \dots, n_M\} \subset \mathbb{R}^d$ , and there is an unique decomposition of the space into regions such that each point within these regions is closer to the node to which the region is associated than to any other in the cloud. This kind of space decomposition is called a Voronoi diagram of the cloud of points and each Voronoi cell is formally defined as (see figure 4):

$$T_I = \{\mathbf{x} \in \mathbb{R}^d : d(\mathbf{x}, \mathbf{x}_I) < d(\mathbf{x}, \mathbf{x}_J) \forall J \neq I\}, \quad (17)$$

where  $d(\cdot, \cdot)$  is the Euclidean distance function.

The dual structure of the Voronoi diagram is the Delaunay triangulation, obtained by connecting nodes that share a common  $(d - 1)$ -dimensional facet. While the Voronoi structure is unique, the Delaunay triangulation is not, there being some so-called *degenerate* cases in which there are two or more possible Delaunay triangulations (consider, for example, the case of triangulating a square in 2D, as depicted in Fig. 4 (right)). Another way to define the Delaunay triangulation of a set of nodes is by invoking the *empty circumcircle* property, which means that no node of the cloud lies within the circle covering a Delaunay triangle. Two nodes sharing a facet of their Voronoi cell are called *natural neighbours* and hence the name of the technique.

In order to define the natural neighbour co-ordinates it is necessary to introduce some additional concepts. The second-order Voronoi diagram of the

cloud is defined as

$$T_{IJ} = \{\mathbf{x} \in \mathbb{R}^d : d(\mathbf{x}, \mathbf{x}_I) < d(\mathbf{x}, \mathbf{x}_J) < d(\mathbf{x}, \mathbf{x}_K) \forall J \neq I \neq K\}. \quad (18)$$

The simplest of the natural neighbour-based interpolants is the so-called Thiessen's interpolant (Thiessen, 1911). Its interpolating functions are defined as

$$\psi_I(\mathbf{x}) = \begin{cases} 1 & \text{if } \mathbf{x} \in T_I \\ 0 & \text{elsewhere.} \end{cases} \quad (19)$$

The Thiessen interpolant is a piece-wise constant function, defined over each Voronoi cell. It defines a method of interpolation often referred to as *nearest neighbour* interpolation, since a point is given a value defined by its nearest neighbour. Although it is obviously not valid for the solution of second-order partial differential equations, it can be used to interpolate the pressure in formulations arising from Hellinger-Reissner-like mixed variational principles such as the one here employed.

Sibson (1980) defined the natural neighbour coordinates of a point  $\mathbf{x}$  with respect to one of its neighbours  $I$  as the ratio of the cell  $T_I$  that is transferred to  $T_x$  when adding  $\mathbf{x}$  to the initial cloud of points to the total volume of  $T_x$ . In other words, if  $\kappa(\mathbf{x})$  and  $\kappa_I(\mathbf{x})$  are the Lebesgue measures of  $T_x$  and  $T_{xI}$  respectively, the natural neighbour coordinates of  $\mathbf{x}$  with respect to the node  $I$  is defined as

$$\phi_I(\mathbf{x}) = \frac{\kappa_I(\mathbf{x})}{\kappa(\mathbf{x})}. \quad (20)$$

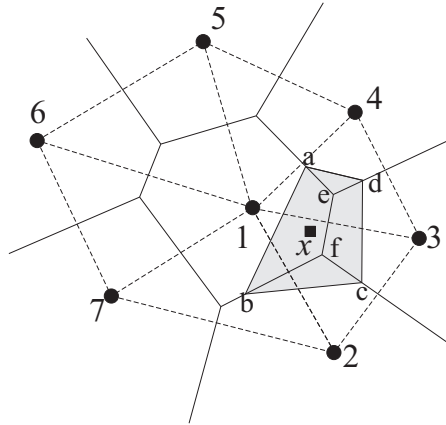


Fig. 5. Definition of the Natural Neighbour coordinates of a point  $\mathbf{x}$ .

In Fig. 5 the shape function associated to node 1 may be expressed as

$$\phi_1(\mathbf{x}) = \frac{A_{abfe}}{A_{abcd}}. \quad (21)$$

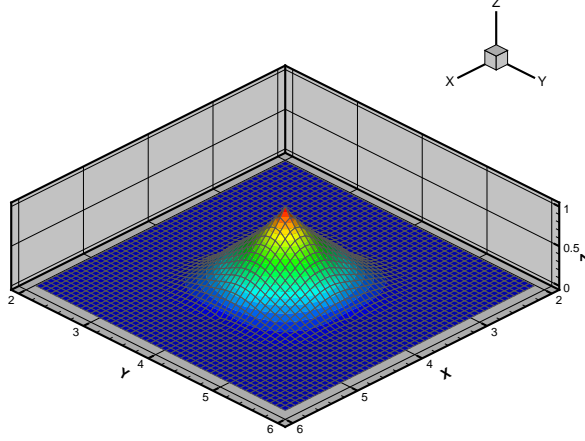


Fig. 6. Typical Sibson function  $\phi(\mathbf{x})$ .

It is straightforward to prove that NE shape functions (see Fig. 6) form a partition of unity (Babuška and Melenk, 1997), as well as some other properties like positivity (i.e.,  $0 \leq \phi_I(\mathbf{x}) \leq 1 \quad \forall I, \forall \mathbf{x}$ ) and strict interpolation:

$$\phi_I(\mathbf{x}_J) = \delta_{IJ}. \quad (22)$$

Recently, Hiyoshi and Sugihara (1999) have generalised the form of natural neighbour interpolants. One different type of interpolation has attracted the interest of researchers, since it is slightly faster to compute, although gives less smooth interpolations. It has received the name of *Laplace* interpolant.

Consider the introduction of the point  $\mathbf{x}$  in the cloud of nodes. Due to this introduction, the Voronoi diagram will be altered, affecting the Voronoi cells of the natural neighbours of  $\mathbf{x}$ . The Laplace interpolant is defined by using geometrical entities of one dimension less than the original space under consideration. If we define the cell intersection  $t_{IJ} = \{\mathbf{x} \in T_I \cap T_J, J \neq I\}$  (note that  $t_{IJ}$  may be an empty set) we can define the value

$$\alpha_J(\mathbf{x}) = \frac{|t_{IJ}|}{d(\mathbf{x}, \mathbf{x}_J)}. \quad (23)$$

Thus, the point  $\mathbf{x}$  shape function value with respect to node 4 in Fig. 7 is defined as

$$\phi_4^{ns}(\mathbf{x}) = \frac{\alpha_4(\mathbf{x})}{\sum_{J=1}^n \alpha_J(\mathbf{x})} = \frac{s_4(\mathbf{x})/h_4(\mathbf{x})}{\sum_{J=1}^n [s_J(\mathbf{x})/h_J(\mathbf{x})]}, \quad (24)$$

where  $s_J$  represent the length of the Voronoi segment associated to node  $J$  and  $n$  represents the number of natural neighbours of the point under consideration,  $\mathbf{x}$ .

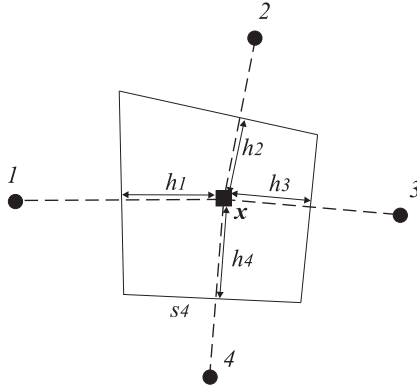


Fig. 7. Definition of non-Sibsonian coordinates.

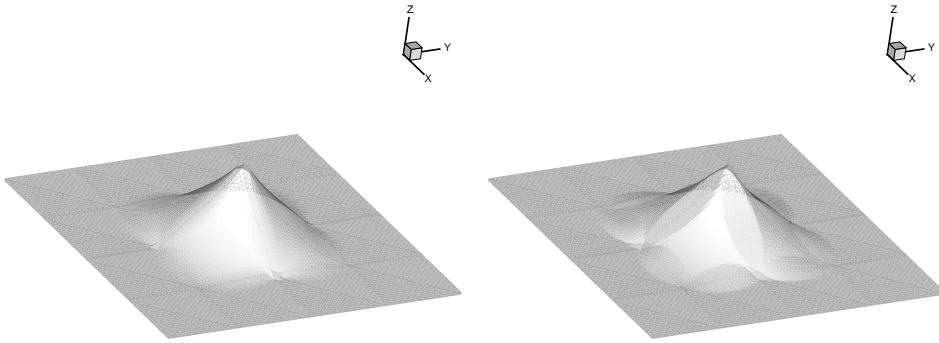


Fig. 8. Comparison of Sibson (a) and Laplace (b) shape functions.

Derivatives of the Laplace shape function are not defined along the edges of the Delaunay triangles that lie inside its support (see the work by Sukumar *et al.* (2001)). For the purposes of the work here presented, a mixed Thiessen-Laplace approximation for pressure and velocity, respectively, has been considered.

Laplace interpolants have some remarkable properties that help to construct the trial and test functional spaces of the Galerkin method (see Hiyoshi and Sugihara (1999) for proofs of these properties). Besides properties like continuity and smoothness (everywhere except at the nodes for Sibson interpolants and at some other lines of zero measure for the Laplace interpolant), Sibson and Laplace interpolants possess linear completeness (i.e., exact reproduction of a linear field). A comparison of Sibson and Laplace shape functions for the same regular lattice of points is done in Fig. 8.

Sibson and Laplace interpolants can also reproduce linear functions exactly along convex boundaries. This is in sharp contrast to the vast majority of meshless methods. In addition, in (Cueto *et al.*, 2000) (Yvonnet *et al.*, 2004) distinct methods of imposing linear displacement fields along non-convex boundaries were developed.

If higher-order Natural Element approximations are needed, the approach presented in González *et al.* (2007) allows for arbitrary orders of consistency and smoothness.

#### 4.3 Functional approximation and discretisation of the problem

As mentioned before, in the approximation of Eqs. (12) and (13), linear approximation was chosen for velocities and constant pressure per elements, when FE technology was employed.

In the case of Natural Element approximation, velocities were approximated by making use of Laplace interpolation, whereas pressure was assumed constant per Voronoi cell by employing Thiessen interpolation. The choice of Laplace instead of Sibson interpolation is dictated by the compromise between accuracy and computational cost, as studied in Alfaro *et al.* (2007).

#### 4.4 Tracking of the domain

Finally, in order to track the evolution of the free-surface of the domain, shape constructors (in particular,  $\alpha$ -shapes, see (Edelsbrunner and Muecke, 1994)) were employed. This allows us to proceed without the need of storing information about the boundary. At each time step, triangles belonging to the boundary are found by the method.

$\alpha$ -shapes define a one-parameter family of shapes  $\mathcal{S}_\alpha$  (being  $\alpha$  the parameter), ranging from the “coarsest” to the “finest” level of detail.  $\alpha$  can be seen, precisely, as a measure of this level of detail. This means that all details of size less than  $\alpha$  will be ignored in the geometry of the domain. This is a common practice in many conversions from CAD models (very often geometrically “exact”) to FEM models, in which very small features of the geometry are ignored from a mechanical point of view.

In order to clarify the before presented concepts, consider some examples of  $\alpha$ -shapes computed from a cloud of points corresponding to the simulation of two-dimensional extrusion process. We restrict ourselves to geometrical concepts only.

Consider the extrusion example shown in Fig. 9, where the contour plot of equivalent plastic strain rate is depicted. The key idea of the method here proposed is to extract the shape of the domain at each time step by invoking the concept of  $\alpha$ -shape of the cloud. The  $\alpha$  parameter will be obtained by geometrical considerations. In this case the radius at the inlet of the die, for

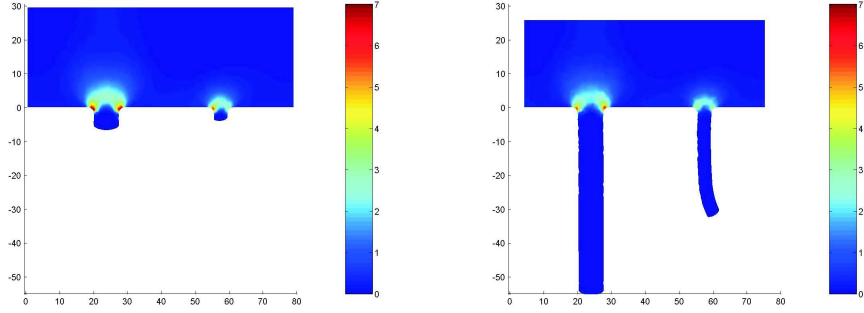


Fig. 9. Two snapshots of a two-dimensional simulation of an extrusion process. Equivalent plastic strain rate is depicted.

instance, seems to be the smallest level of detail up to which the domain (i.e., the billet) must be represented. In order to appropriately represent this value, the nodal distance  $h$  must be accordingly chosen.

In Fig. 10 some members of the family of  $\alpha$ -shapes of the cloud of points in its final configuration (corresponding to Fig. 9(b)) are depicted. In Fig. 10(a) the member for  $\alpha = 0$ , i.e., the cloud of points itself, is shown. Note how, as  $\alpha$  is increased, the number and size of the simplexes (in this case, triangles) that belong to the shape is increasing. For  $\alpha = 1.0$  we obtain an appropriate shape for the cloud. Note, however, that this is not an exact value to be determined at each time step. Since the number of  $\alpha$ -shapes is finite, there generally exists an interval of valid  $\alpha$  values for a single shape. Finally, by increasing the  $\alpha$  value, we arrive to the convex hull of the cloud of points (Fig. 10(f)).

## 5 Comparison between numerical and experimental predictions

### 5.1 Requested load during the process

The predicted punch load, as well as the experimental one, is reported in Fig. 11. Some underestimation of the punch load is obtained if friction is not taken into account, as expected. This is obvious, but still a good qualitative agreement is obtained. Improved results are obtained, however, if we consider in the simulation the viscoplastic friction model, detailed in Section 2.2. An overestimation of the punch load is obtained, however, at the initial time steps of the simulation. This has been repeatedly observed, since numerical simulations do not take into account imperfections in the material, voids, etc., that make the actual experiments to occur with lower loads at the initial stages of extrusion.

After 3 mm of stroke displacement, FEM simulation (without considering

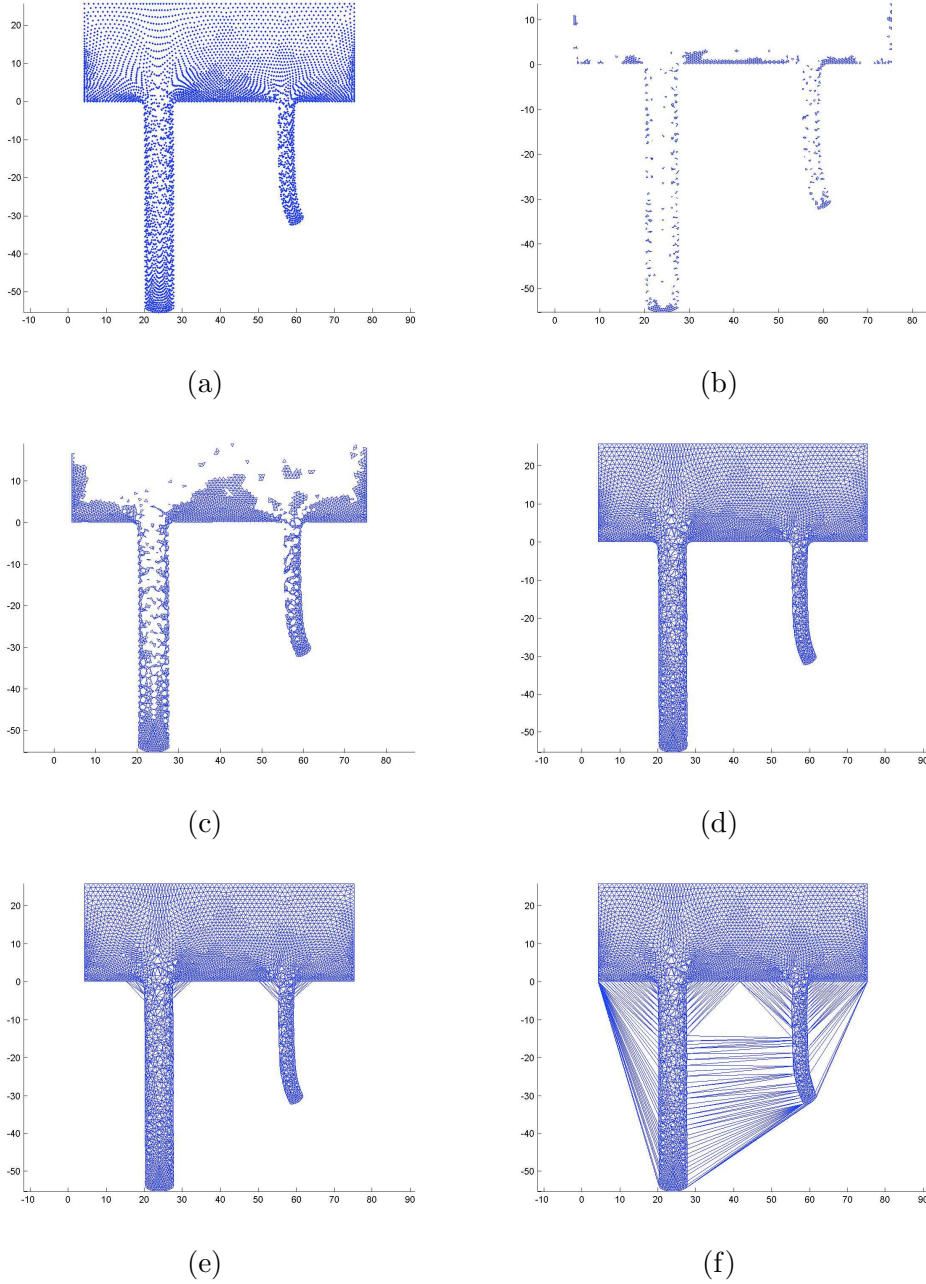


Fig. 10. Some members of the family of  $\alpha$ -shapes of the cloud of points used in the extrusion example. (a)  $\mathcal{S}_0$  (the cloud of points) (b)  $\mathcal{S}_{0.3}$  (c)  $\mathcal{S}_{0.5}$  (d)  $\mathcal{S}_{1.0}$  (e)  $\mathcal{S}_{1.5}$  and (f)  $\mathcal{S}_{\infty}$  (the convex hull of the set)

friction) was not able to converge any more, due to the distortion of the mesh together with the incompressibility and the nonlinear material model. Note that we are not allowing remeshing, neither in the FEM nor in the NEM simulations. This means that the usual practice of generating a new mesh, with improved quality tetrahedra, and projecting old variables to the new mesh, has not been accomplished. This is quite a fictitious procedure, but we tried to avoid the introduction of the well-known numerical diffusion associated to

remeshing.

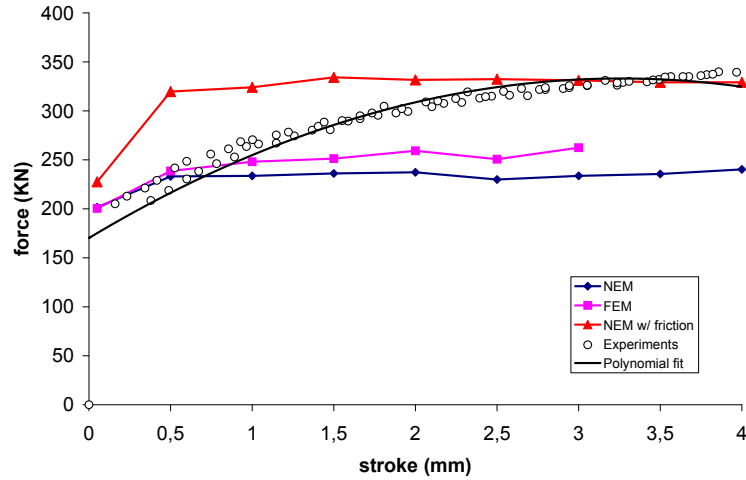


Fig. 11. Evolution of the punch load. Results with the FEM and NEM without friction, NEM with friction, and experiments. The best polynomial fit to the experimental results is also shown.

## 5.2 Shape of the extrudate

About 25 mm of extrudate were simulated with NEM. In order to verify the accuracy of the prediction, the deviation of the profile from the straight line is compared to that of the experiments and the FEM simulation. It is possible to verify the sufficiently good prediction of the distortion of the profile induced by the die asymmetry (see Fig. 12).

Again, taking into account the friction, the obtained results fit very well to experimental data. In addition, comparing the results for 3 mm of stroke displacement (Fig. 13), FEM (without friction) and NEM results are very similar. Note however that at this displacement value FEM simulation could not achieve convergence due to mesh distortion. It is then concluded that the friction has an important effect on the determination of punch load, as expected, but not so much in the shape of the extrudate.

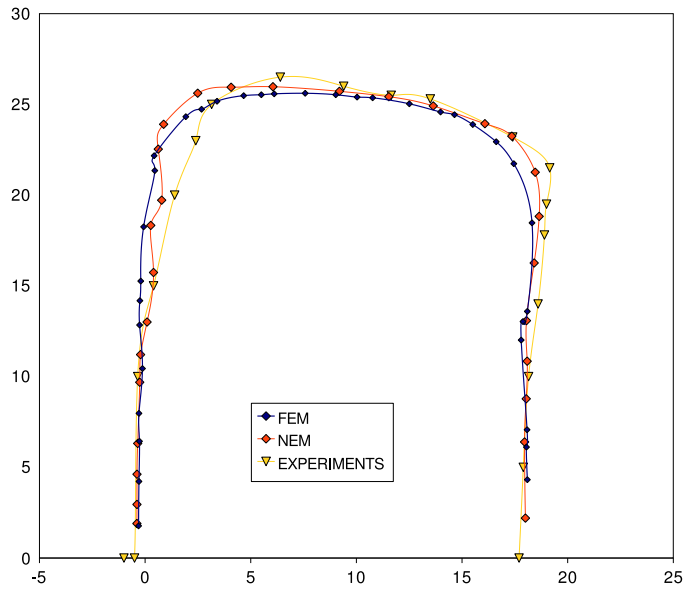
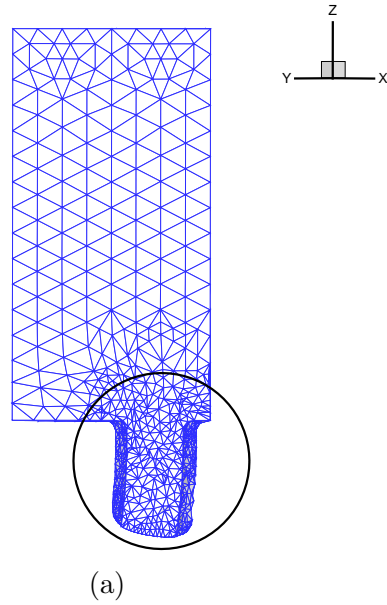


Fig. 12. Deviation due to die misalignment. (a) zone measured (b) profile of the extrudate.

### 5.3 Pressure at the bottom of the die

Another interesting comparison was carried out with reference to the predicted pressure on the bottom die, along the symmetry plane, from point A to point B, according to the following Fig. 14. In this case, no experimental

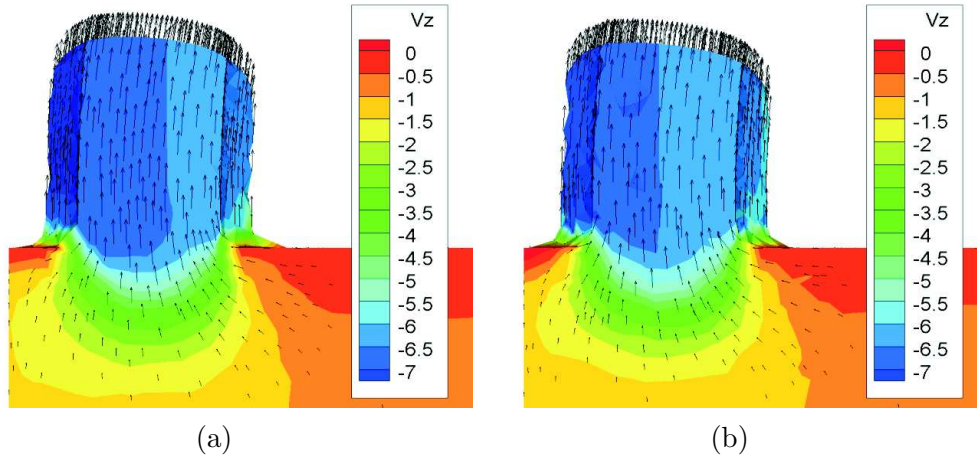


Fig. 13. Exit velocity distribution: FEM (a) and NEM (b).

measurements were available, so only numerical predictions were compared.

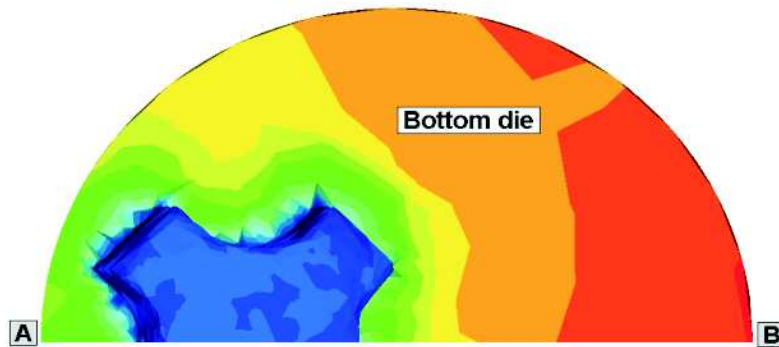


Fig. 14. Pressure analysis section on the bottom die.

Figure 15 shows the predicted pressure distribution. No friction was considered in this particular comparison in order to simplify the analysis. In this case the predicted pressure smoothness is better in the NE case. The FE results show some spurious oscillations, which are well-know in the FE community. The NEM, however, despite the simple formulation employed, does not show spurious oscillations. A more detailed discussion on the performance of mixed NEM approximations for incompressible materials can be found in (González *et al.*, 2004). Another important fact is that the FE shows some spurious pressure peaks due to the obvious distortion of the mesh. This is shown in Fig. 16.

The influence of the quality of the mesh on the results is highlighted in Fig. 17. In it, the simulation was ran by using NEM until a given time step. It was then stopped and one time step more was accomplished by means of both FEM and NEM. In this way, a direct comparison of the results and the influence of the technique on them can be achieved. Equivalent strain rate results are depicted. Note the spurious concentration of strain rate near a zone with distorted elements, which does not appear in the NEM results. In

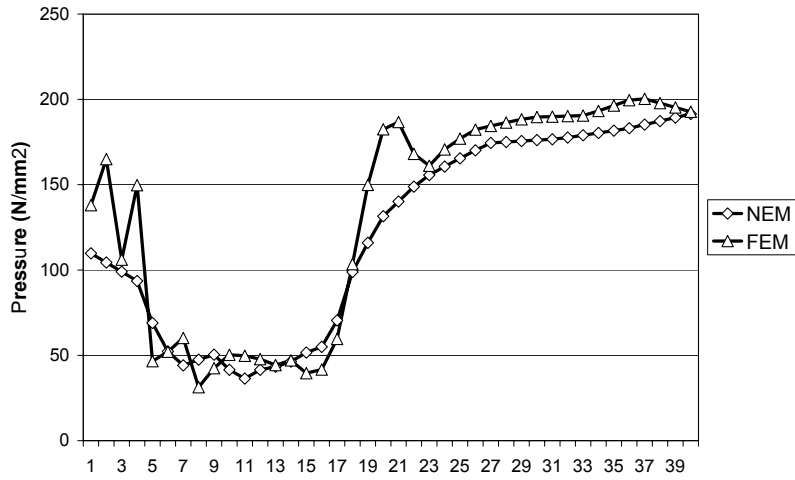


Fig. 15. Pressure on the bottom die, along the A-B line.

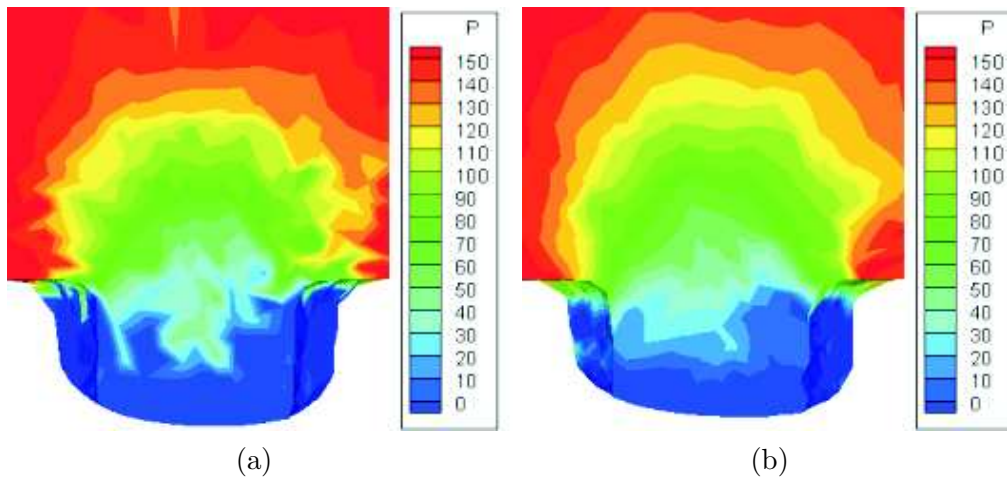


Fig. 16. Spurious pressure distribution obtained in the FE formulation during the simulation. FE results (a) and NE results (b) .

addition, overall FEM strain rate values are somewhat higher than those of the NEM simulation.

## 6 Conclusions

A first comparison between a FEM and a NEM formulation for the numerical simulation of extrusion processes was proposed in the paper, focusing the attention on the extrusion of a cross shaped component. At the end of this

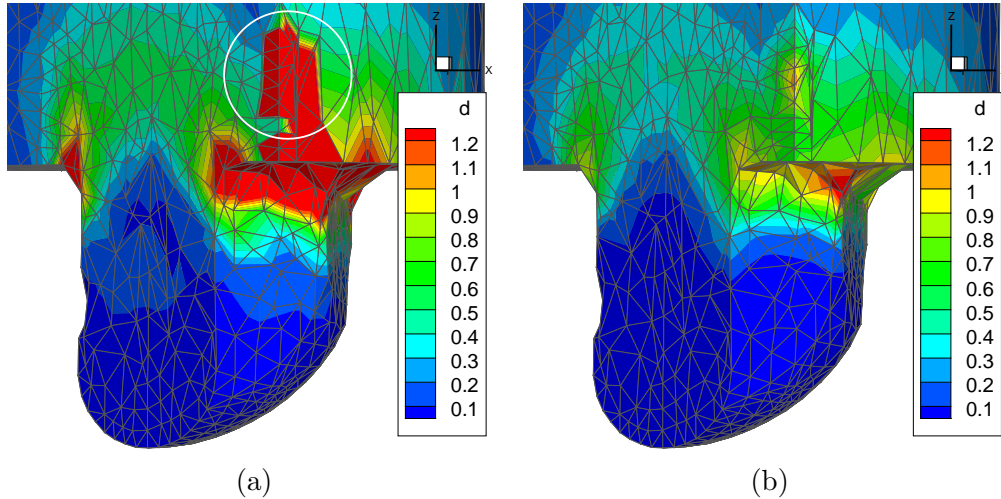


Fig. 17. Spurious equivalent strain rate distribution obtained in the FE formulation during the simulation. FE results (a) and NE results (b). The highlighted zone shows the anomalous values.

work some conclusions can be traced:

- Meshless methods, despite their relative lower state of development, show promising capabilities in the simulation of forming processes with large deformations.
- NEM is today computationally more expensive because it needs more time in calculating the shape functions and, being a very novel approach, a relevant optimisation work remains to be done.

The computational cost of the NEM has been estimated in about four times that of the FEM in some of our previous works (Alfaro *et al.*, 2007). Nevertheless, this cost is negligible, if compared to the cost of performing iterations in the Newton-Raphson loop. Very efficient algorithms have been developed in order to alleviate this computational cost (the natural neighbour search, for instance, see the work by Alfaro *et al.* (2007)). At this moment, we believe that the NEM is a competitive technique in terms of CPU hours, if we deal with highly non-linear problems.

We believe that the use of meshless methods in the simulation of extrusion processes can be especially interesting for the extrusion of hollow profiles. Such processes involve a complex flow through the die, with melting fronts of material at the exit. Eulerian (fixed mesh) or ALE approaches can handle this type of flows with difficulties due to the complex geometry of the extrudate. This constitutes our current effort of research.

At this moment NEM formulation is not implemented in any commercial program even if it can supply a decisive answer to the need of simulating some specific problems, like the mentioned extrusion of hollow components. We believe

that the NEM constitutes nowadays an appealing choice for the simulation of some complex phenomena, like those involving free surfaces, as mentioned before, or the need of an accurate description of evolving fronts.

## Acknowledgements

The authors would like to thank Mr. F. Pulice for his contribution in the development of the experimental equipment.

## References

- Alfaro, I., Yvonnet, J., Cueto, E., Chinesta, F., and Doblaré, M. (2006a). Meshless methods with application to metal forming. *Computer Methods in Applied Mechanics and Engineering*, **195**, 6661–6675.
- Alfaro, I., Bel, D., Cueto, E., Doblaré, M., and Chinesta, F. (2006b). Three-dimensional simulation of aluminium extrusion by the alpha-shape based natural element method. *Computer Methods in Applied Mechanics and Engineering*, **195(33–36)**, 4269–4286.
- Alfaro, I., Yvonnet, J., Chinesta, F., and Cueto, E. (2007). A study on the performance of Natural Neighbour-based Galerkin Methods. *International Journal for Numerical Methods in Engineering*, **7(12)**, 1436–1465.
- Babuška, I. and Melenk, J. M. (1997). The partition of unity method. *International Journal for Numerical Methods in Engineering*, **40**, 727–758.
- Bonet, J. and Kulasegaram, . (2000). Correction and stabilization of smooth particle hydrodynamics methods with applications in metal forming simulations. *International Journal for Numerical Methods in Engineering*, **47-6**, 1189–1214.
- Chen, J. S., Roque, C. M. O. L., Pan, C. H., and Button, S. P. (1998). Analysis of metal forming process based on meshless method. *Journal of Materials Processing Technology*, **80-1**, 642–646.
- Chenot, J.-L., Fourment, L., and Mocellin, K. (2002). Numerical treatment of contact and friction in fe simulation of forming processes. *Journal of Materials Processing Technology*, **125–126**, 45–52.
- Cueto, E., Doblaré, M., and Gracia, L. (2000). Imposing essential boundary conditions in the Natural Element Method by means of density-scaled  $\alpha$ -shapes. *International Journal for Numerical Methods in Engineering*, **49-4**, 519–546.
- Edelsbrunner, H. and Muecke, E. (1994). Three dimensional alpha shapes. *ACM Transactions on Graphics*, **13**, 43–72.
- González, D., Cueto, E., and Doblaré, M. (2004). Volumetric locking in Natu-

- ral Neighbour Galerkin methods. *International Journal for Numerical Methods in Engineering*, **61(4)**, 611–632.
- González, D., Cueto, E., and Doblaré, M. (2007). Higher-order Natural Element Methods: towards an isogeometric meshless method. *International Journal for Numerical Methods in Engineering*, **accepted for publication**.
- Hiyoshi, H. and Sugihara, K. (1999). Two generalizations of an interpolant based on Voronoi diagrams. *International Journal of Shape Modeling*, **5(2)**, 219–231.
- Sibson, R. (1980). A Vector Identity for the Dirichlet Tessellation. *Mathematical Proceedings of the Cambridge Philosophical Society*, **87**, 151–155.
- Sibson, R. (1981). A brief description of natural neighbour interpolation. In *Interpreting Multivariate Data. V. Barnett (Editor)*, pages 21–36. John Wiley.
- Sukumar, N., Moran, B., and Belytschko, T. (1998). The Natural Element Method in Solid Mechanics. *International Journal for Numerical Methods in Engineering*, **43(5)**, 839–887.
- Sukumar, N., Moran, B., Semenov, A. Y., and Belikov, V. V. (2001). Natural Neighbor Galerkin Methods. *International Journal for Numerical Methods in Engineering*, **50(1)**, 1–27.
- Thiessen, A. H. (1911). Precipitation averages for large areas. *Monthly Weather Report*, **39**, 1082–1084.
- Yvonnet, J., Ryckelynck, D., Lorong, P., and Chinesta, F. (2004). A new extension of the Natural Element method for non-convex and discontinuous problems: the Constrained Natural Element method. *International Journal for Numerical Methods in Engineering*, **60(8)**, 1452–1474.
- Zhou, J., Li, L., and Duszcyk, J. (2003). 3D FEM simulation of the whole cycle of aluminium extrusion throughout the transient state and the steady state using the updated Lagrangian approach. *Journal of Materials Processing Technology*, **134**, 383–397.
- Zienkiewicz, O. C. and Godbolet, P. N. (1974). Flow of plastic and visco-plastic solids with special reference to extrusion and forming processes. *International Journal for Numerical Methods in Engineering*, **8**, 3–16.